SUPPORTING INFORMATION

Positron Annihilation Spectroscopy: A New Frontier for Understanding Nanoparticle-Loaded Polymer Brushes

Guido Panzarasa[†,‡*] *Stefano Aghion,* [§,#,‡] *Guido Soliveri,*[¤] *Giovanni Consolati,*[⊥] *and Rafael Ferragut*[§,#]

[†]Department of Science and Technological Innovation, Università del Piemonte Orientale "Amedeo Avogadro", viale T. Michel 11, 15100 Alessandria, Italy. E-mail: gp4779@gmail.com

[§]LNESS, Department of Physics, Politecnico di Milano, via Anzani 42, 22100 Como, Italy

[#]Istituto Nazionale di Fisica Nucleare, via Celoria 16, 20133 Milano, Italy

[¤]Department of Chemistry, Università degli Studi di Milano, via C. Golgi 19, 20133 Milano, Italy

[⊥]Department of Aerospace Science and Technology, Politecnico di Milano, via La Masa 34, 20156 Milano, Italy

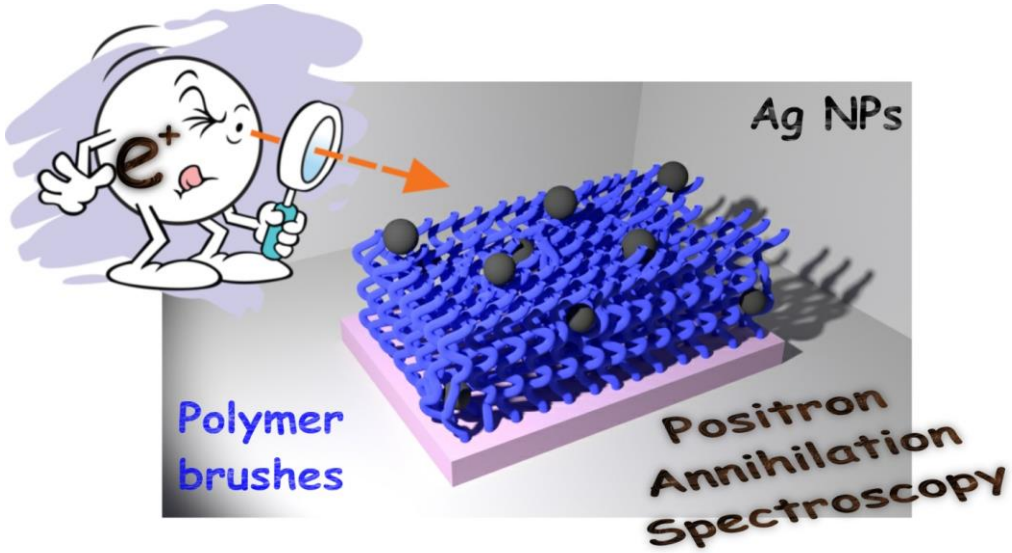

EXPERIMENTAL PROCEDURES

MATERIALS

All the chemicals, unless otherwise stated, were reagent grade, purchased from Aldrich and used as received. Water obtained from a Millipore MilliQ purification system (resistivity ≥ 18.2 MΩ cm^{-1}) was thoroughly used. DMAEMA monomer was filtered through an inhibitor-remover column and stored at –18°C until use. Silicon (100) wafers, single-polished, n type, phosphorus doped, 3 – 6 (Ω cm), with a native oxide layer ca. 1.5 nm thick, were purchased from Ultrasil Corporation. The wafers were cut into substrates of convenient size and cleaned by immersion for 1 h at 100 °C in a piranha solution made of a $3{:}1_{v/v}$ mixture of concentrated sulphuric acid and hydrogen peroxide, respectively (*Caution: hot, concentrated piranha solution is corrosive and dangerous!*). Each substrate was then rinsed extensively with MilliQ water and dried under a nitrogen stream. Glass microscope slides were used as transparent substrates and were treated as described for the silicon substrates.

SYNTHESIS AND GRAFTING OF THE (3-(2-BROMOISOBUTYRAMIDO)PROPYL)TRIETHOXYSILANE (BIB-APTES) ATRP INITIATOR

The synthetic procedure was described in detail in a previous work[1]. Briefly, 7 mL (30 mmol) 3-aminopropyltriethoxysilane (APTES) and 5 mL (36 mmol) triethylamine were dissolved in 50 mL anhydrous THF in a three-necked 100 mL round bottom flask, equipped with a dropping funnel, a nitrogen inlet and a mechanical stirrer, immersed in an ice bath. 4.45 mL (36 mmol) 2-bromoisobutyryl bromide (BIBB) were added dropwise under stirring and the reaction was allowed to continue at room temperature for 3 h. The white solid (triethylammonium bromide) was filtered

off and the volatiles removed at 50 °C using rotavapor. The product was redissolved in anhydrous THF, filtered through silica gel to separate a brown impurity. After evaporation of the solvent, a quantitative yield of a viscous, colorless liquid was obtained and stored at +4 °C.

For the functionalization with BIB-APTES, piranha-cleaned silicon substrates were immersed in a 10 mM BIB-APTES solution in anhydrous toluene for 4 h at 55 °C, left overnight at 30 °C, washed and gently sonicated with toluene, acetone and ethanol and dried with a nitrogen stream. The functionalized substrates were stored at room temperature in the dark until use.

GRAFTING-FROM OF PDMAEMA BRUSHES BY SI-ATRP

Poly(dimethylaminoethyl methacrylate) (PDMAEMA) brushes were grown by means of surface-initiated atom transfer radical polymerization (SI-ATRP) as previously described[2] (Scheme S1). Briefly, each initiator-functionalized substrate was placed in a nitrogen-purged Schlenck flask and covered with 5 mL of a polymerization mixture prepared as follow. In a nitrogen-purged Schlenck flask 0.312 g (2.0 mmol) of bipyridyl and 0.144 g (1.0 mmol) of copper(I) bromide were dissolved in 6 mL of a 4:1 v/v methanol-water mixture previously degassed by bubbling nitrogen. 14 mL (83 mmol) of degassed DMAEMA were added and the mixture was stirred under nitrogen to obtain a homogeneous solution. For polymerizations with added deactivator the polymerization mixture contained also 11 mg (0.05 mmol) of copper(II) bromide. Polymerization proceeded at 30 °C for different times to control the brush thickness. After polymerization the samples were rinsed extensively with ethanol, gently sonicated in the same solvent and dried under a nitrogen stream.

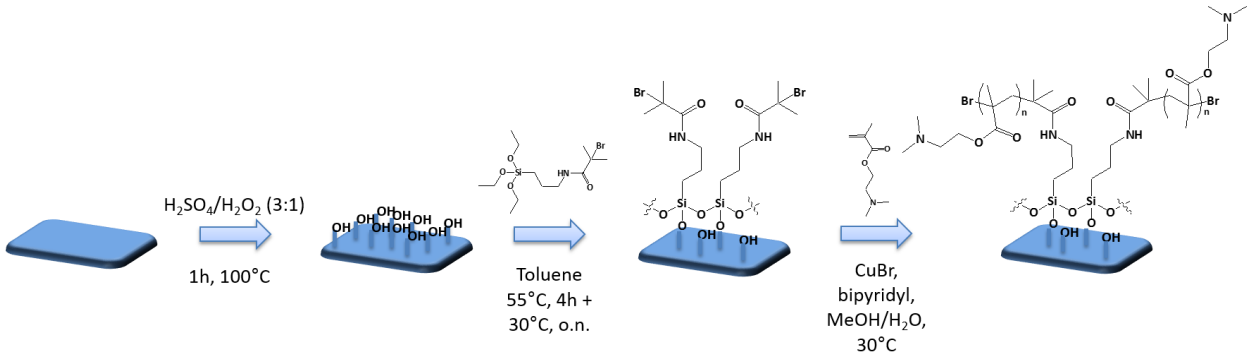

Scheme S1. Synthesis of grafted PDMAEMA brushes by surface-initiated ATRP.

SYNTHESIS AND INCORPORATION OF SILVER NANOPARTICLES INTO PDMAEMA BRUSHES

An aqueous suspension of negatively charged silver nanoparticles were synthesized according to a reported procedure[3,4]. Briefly, 0.15 g (0.88 mmol) of silver nitrate were dissolved in 25 mL of water and this solution was added under stirring to a solution of 0.50 g (1.7 mmol) of trisodium citrate and 0.25 g of poly(vinylpyrrolidone) (PVP10, $M_w \sim 10000$ g mol^{-1}) in 125 mL of water. The resulting solution was poured in a three-necked, round-bottomed 250 mL flask equipped with a mechanical stirrer and a dropping funnel. The solution was cooled in an ice bath and an ice-cooled solution of sodium borohydride, obtained by dissolving 12 mg (0.32 mmol) of solid in 30 mL of water, was added dropwise under stirring. The resulting dark brown suspension was left under stirring for 5 minutes after the addition, aged at + 4 °C for 24 hours before use and stored in the dark at that temperature. HR-TEM showed particles with an average diameter of 11 ± 1 nm with high crystallinity and sharp size distribution. The aqueous particle suspension displayed the characteristic surface plasmon resonance peak at around 400 nm associated with silver nanoparticles of dimensions lower than 30 nm. Zeta potential measurements confirmed that the particle surface was negatively charged (-30 ± 3 mV) due to strong adsorption of citrate molecules.

PDMAEMA brushes were immersed into aqueous 0.1 M HNO_3 for 1 h to allow complete protonation. The brushes were then washed with water, dried with a stream of nitrogen and dipped in the silver nanoparticle suspension for 10 min under gentle stirring. Eventually the particle-loaded brushes were washed with water, sonicated in the same solvent for 5 min to detach loosely-bound particles and dried under a nitrogen stream.

CHARACTERIZATION TECHNIQUES (OTHER THAN PAS)

Brush thickness was routinely measured using a Filmetrics F20 reflectometer. Each data was the result of three measurements on different spots of a same sample. Scanning electron microscopy (SEM) was performed, on samples fixed on conducting carbon tape, using a Jeol JSM 7600f Schottky Field Emission Scanning Electron Microscope. High resolution transmission electron microscopy (TEM) was performed using a JEM 2010 equipped with a LAB6 electron gun (beam energy 200 keV) and a Gatan CCD camera allowing high resolution imaging. Atomic force microscopy (AFM) pictures were acquired on a Ntegra Aura AFM (NT-MDT) device in tapping mode, with NSC35/AIBS tips (μmasch). X-ray reflectivity (XXR) measurements were performed on a Panalytical X'Pert α1 instrument using a thin film attachment, in the 2θ range of 0–7° at 0.001° (2θ) s^{-1}, operating at 1.6 kW power under Cu Kα radiation (λ = 1.5416 Å). Experimental spectra were fitted using the Panalytical software *Reflectivity*. UV-visible absorption spectroscopy was performed using a Jasco V-630 spectrophotometer. Zeta potential was measured using a Malvern Zetasizer APS Nano. Water contact angle measurements were performed using a Krüss Easy Drop Standard with DSA1 software. A 2 μL-drop of HPLC-grade water was deposited and the contact angle measured after 5 s. Each WCA value is the average of at least three measurements performed on different spots of a same sample. X-ray photoelectron spectroscopy (XPS) analyses were performed using a PHI-5500–Physical Electronics spectrometer, equipped with a monochromatized source with aluminium anode

(Kα = 1486.6 eV) operating at a 200 W of applied power. Samples were placed in UHV (10^{-9} Torr) and irradiated with 200 kV X-rays, survey scans were recorded at a 23.50 eV pass energy, 0.2 s time per step and 0.5 eV energy-step. XPS spectra were collected at takeoff angles of 45°. The analysis area was 0.8 mm^2 and the depth was within 10 nm. The spectrometer was calibrated assuming the Ag(3d 5/2) binding energy (BE) at 368.3 eV with respect to the Fermi-level and the measured full width half maximum (FWHM) was 0.46 eV. The quantitative analysis data were reported as atomic percentage of elements and the normalization was performed without including hydrogen.

ESTIMATION OF THE BRUSH PARAMETERS

Using a surface density of initiator molecules σ_i = 0.4 nm^{-2} the chain average molecular mass M_n was estimated, assuming that all initiator sites induced polymerization and grew with an identical rate, according to eq. S1:

$$M_n = \frac{N_A h d}{\sigma_i} = \frac{N_A \Gamma}{\sigma_i} \quad \text{(S1)}$$

where N_A is Avogadro's number, h and d the thickness and density of the brushes, respectively and Γ the surface coverage. Since the fraction of initiator molecules that induces simultaneous polymer growth is undoubtedly less than unity, it should be noted that the M_n values of the PDMAEMA brushes listed in Table S1 represent a lower limit.

Sample	Polymerization time *h*	Thickness *nm*	Density *g cm^{-3}*	Surface coverage *μg cm^{-2}*	Estimated M_n *g mol^{-1}*
1	0.25	21	1.5	3	47423
2	0.5	36	1.8	6	97556
3	2	63	1.8	11	170724

Table S1. XRR values obtained for pristine PDMAEMA brushes.

Sample	Thickness (before AgNPs) *nm*	Density (before AgNPs) *g cm^{-3}*	Initiator layer-brush interface roughness (before AgNPs) *nm*	Brush-air interface roughness (before AgNPs) *nm*
Ag1	22 (21)	1.49 (1.5)	0.3 (0.32)	1.4 (3)
Ag2	36 (36)	0.9 (1.8)	0.25 (0.25)	0.26 (1.8)
Ag3	60 (63)	1.34 (1.8)	0.4 (0.4)	2.6 (1.1)

Table S2. XRR values obtained for silver nanoparticle-loaded PDMAEMA brushes.

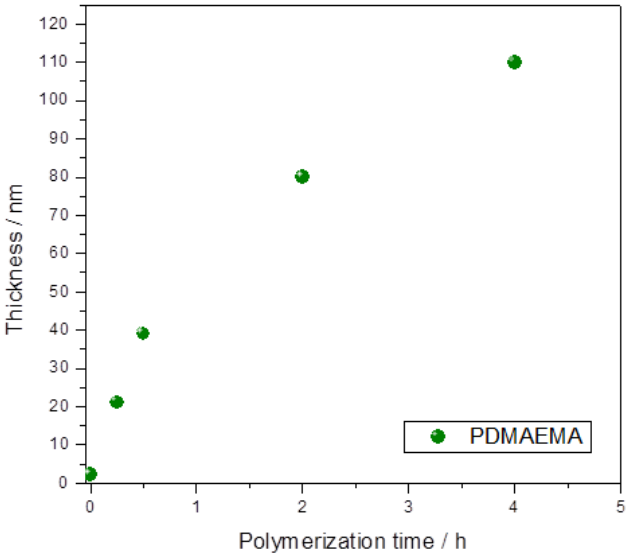

Figure S1. Polymerization kinetics for PDMAEMA brushes obtained by SI-ATRP.

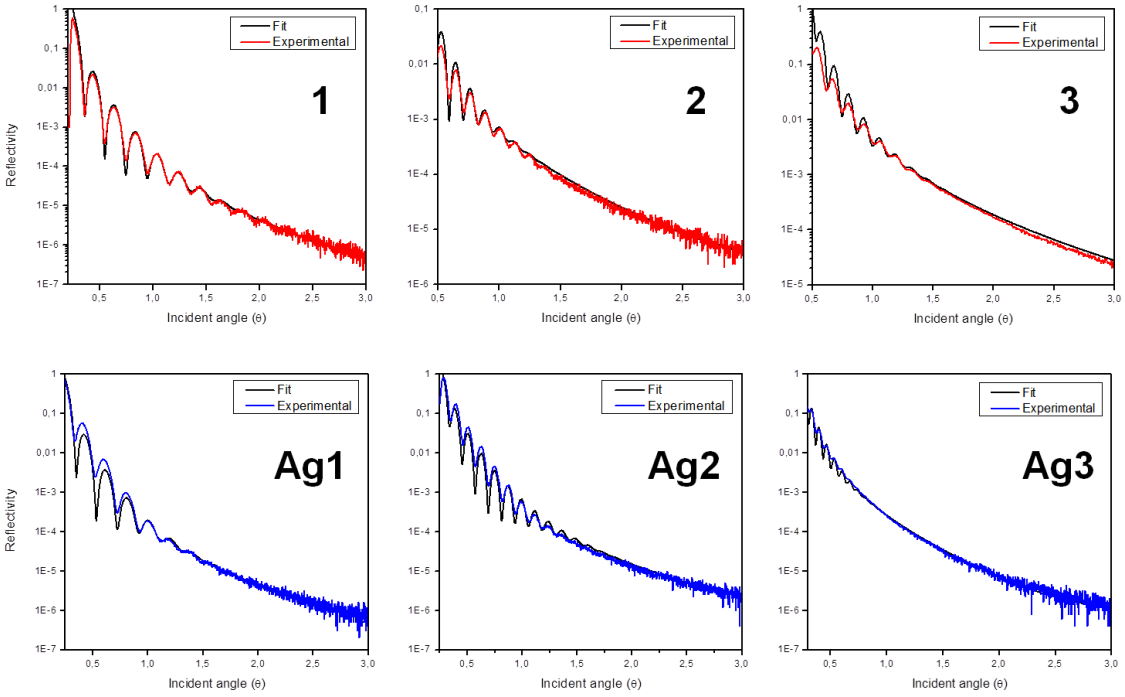

Figure S2. XRR spectra of PDMAEMA brushes before (red lines) and after (blue lines) incorporation of silver nanoparticles along with the fitted curves (black lines). The spectra are normalized.

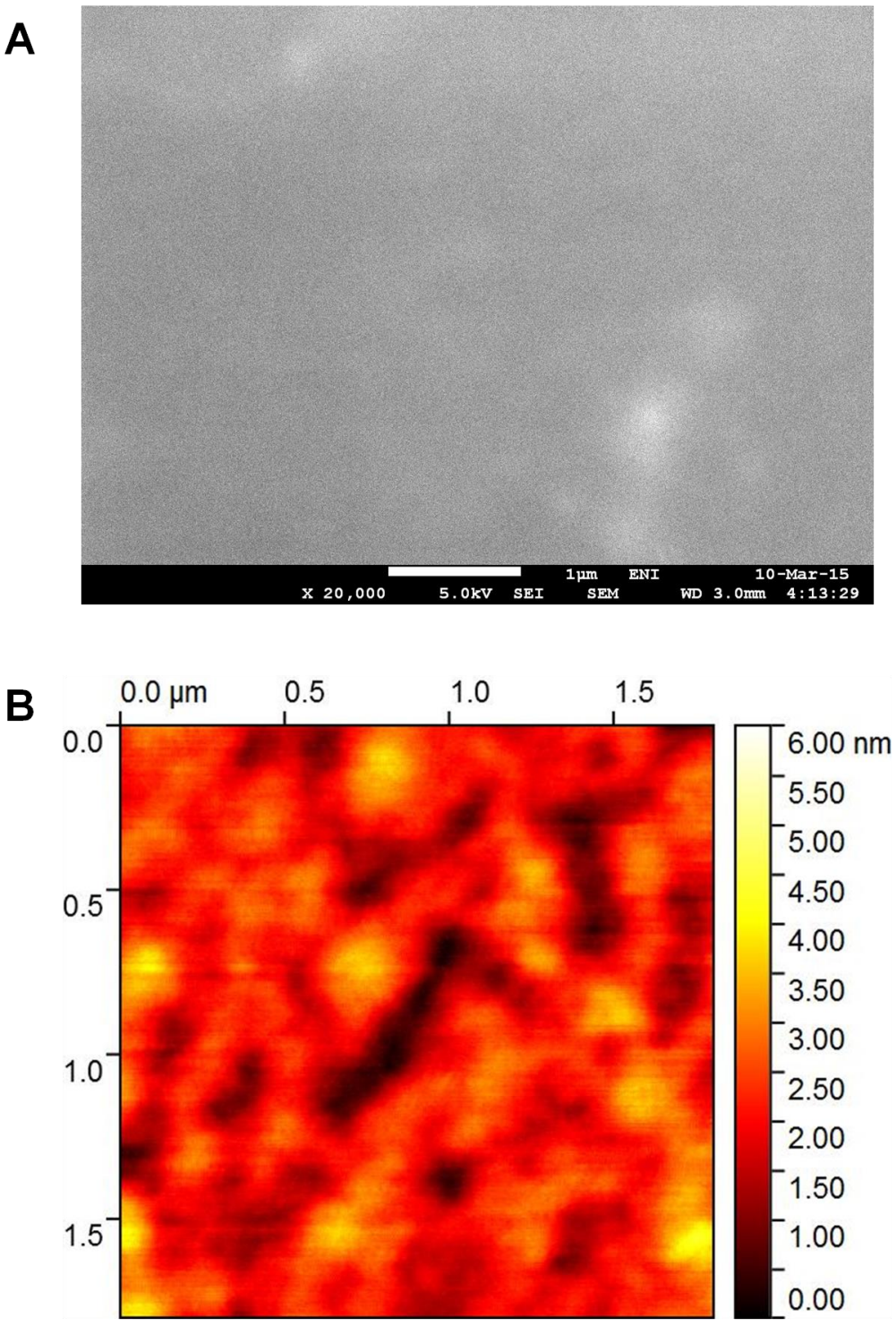

Figure S3. A) SEM and B) AFM images of pristine PDMAEMA brushes (roughness, rms 0.79 nm).

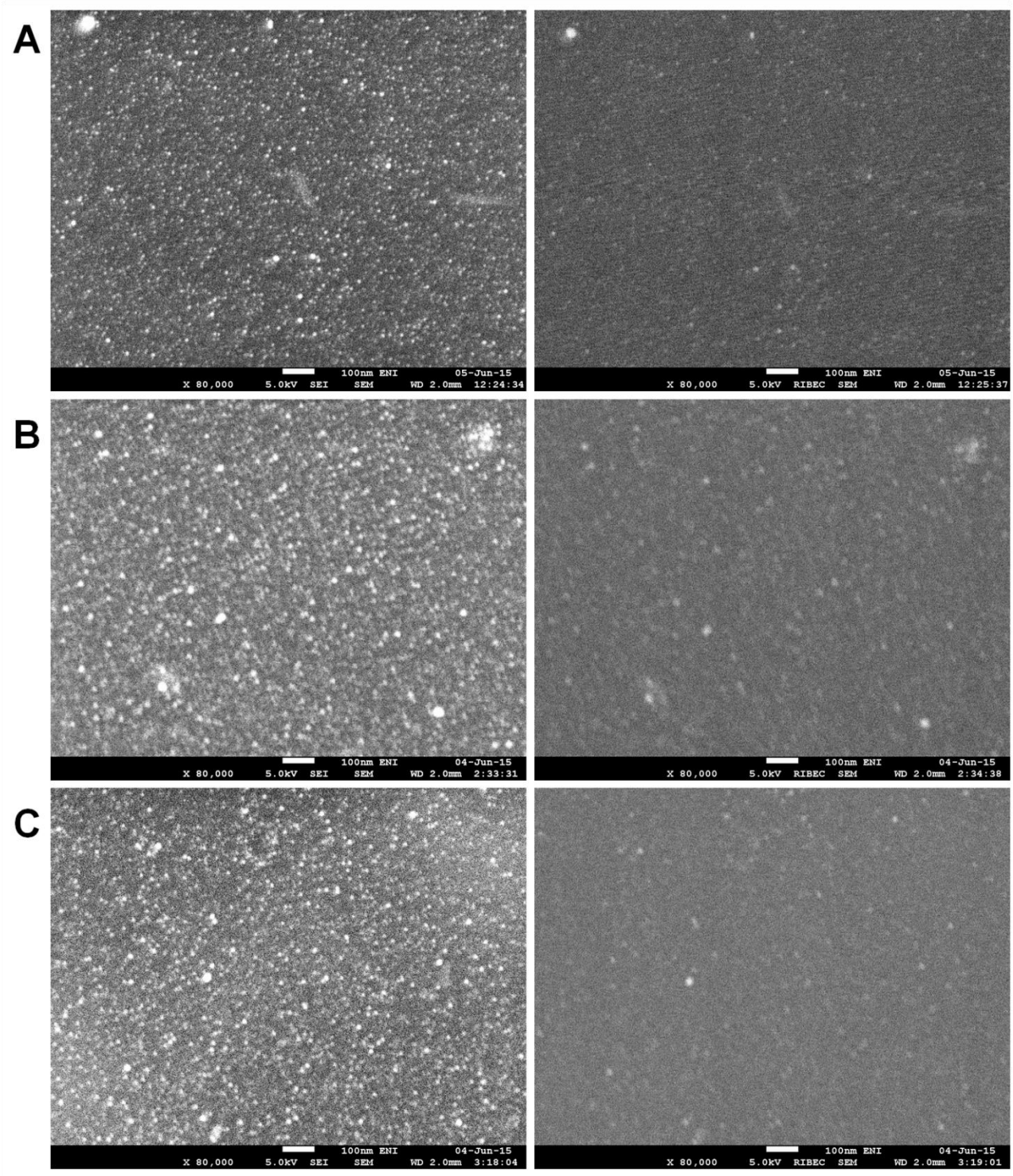

Figure S4. SEM images (left: topographic images; right: backscattered electrons) of silver nanoparticle-loaded polymer brushes: A) **Ag1**, B) **Ag2**, C) **Ag3**.

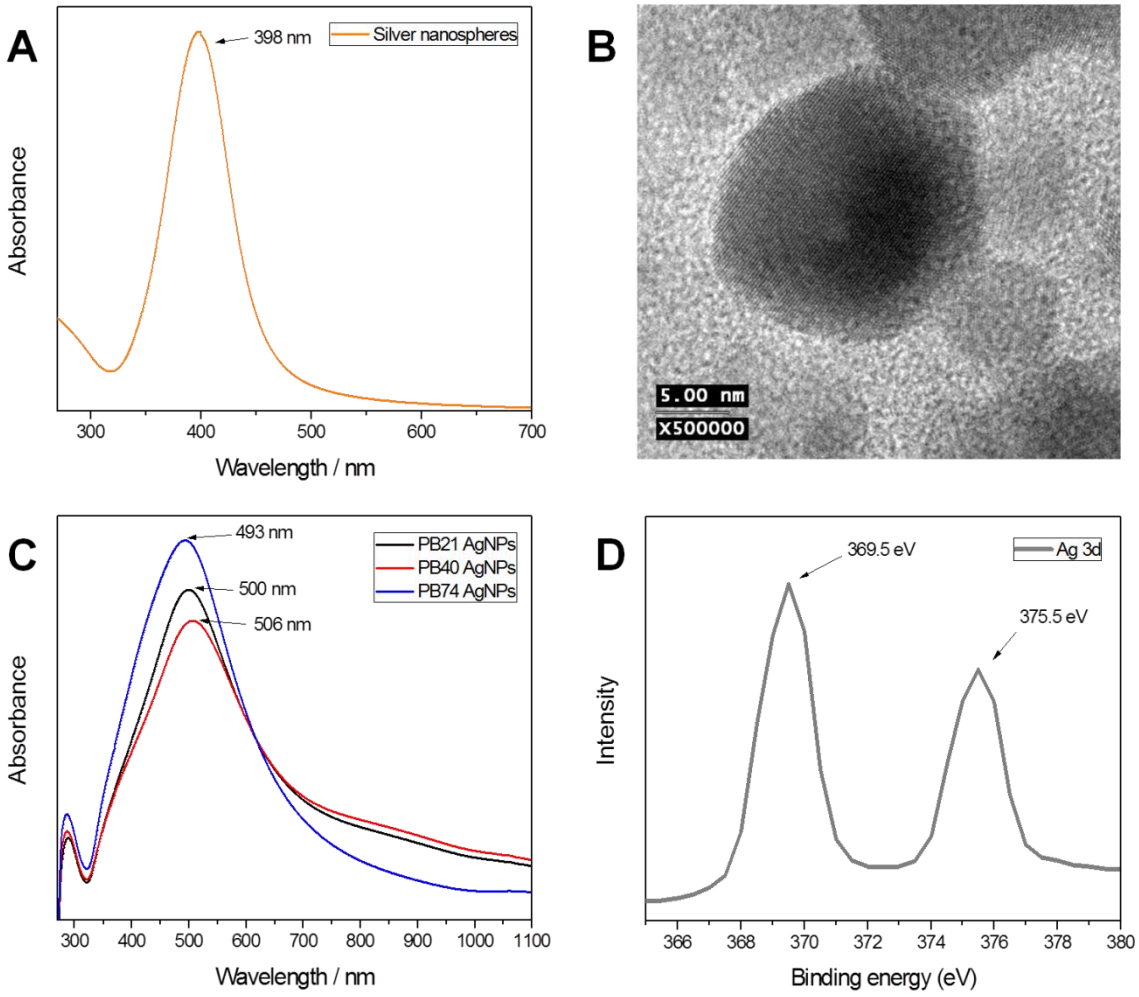

Figure S5. A) UV-vis absorption spectrum of silver nanoparticles (aqueous suspension). B) Representative TEM image of a silver nanoparticle showing high crystallinity: the lattice spacing (ca. 223 pm) corresponds to the (111) planes of a silver fcc cell. C) UV-vis absorption spectra of nanoparticle-loaded polymer brushes. The spectra have been normalized. D) XPS high resolution spectrum showing shifted Ag 3d peaks indicative of Ag^{+} species.

The original aqueous suspension of silver nanoparticles displayed a sharp peak centered at 400 nm which is characteristic of monodisperse silver nanospheres with a mean diameter < 30 nm and is the fingerprint of a dipole surface plasmon resonance (SPR). SPR is known to be highly sensitive to variations of the particle aggregation state and of the refractive index of particle-

surrounding medium. Three brush samples (**PB21 AgNPs**, **PB40 AgNPs** and **PB74 AgNPs**) with different thicknesses (21, 40 and 74 nm, respectively) were grown on glass substrates and loaded with silver nanoparticles. The UV-visible absorption spectra of the resulting particle-brush nanocomposites (Figure S5B) revealed a broader, tailed and red-shifted band compared to that displayed by "free" nanoparticles. This could be a consequence of both steric and optical effect. Brush-embedded silver nanoparticles are closer to each other due also to the collapse of polymer chains upon drying. The particles experience also a significant variation in the refractive index of the surrounding medium, passing from water (n_{water} = 1.33) to PDMAEMA ($n_{PDMAEMA}$ = 1.52).

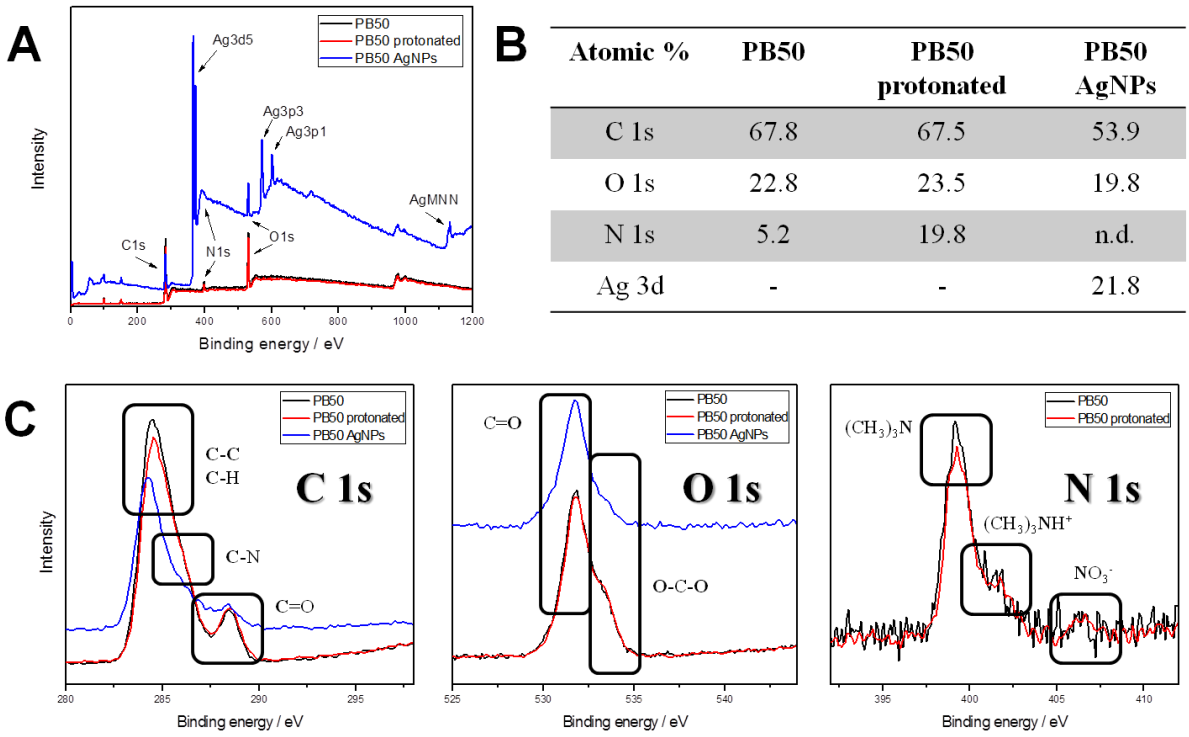

Atomic %	PB50	PB50 protonated	PB50 AgNPs
C 1s	67.8	67.5	53.9
O 1s	22.8	23.5	19.8
N 1s	5.2	19.8	n.d.
Ag 3d	-	-	21.8

Figure S6. XPS spectra for 50 nm-thick PDMAEMA brushes before and after protonation, after loading of silver nanoparticles. A) survey, B) calculated atomic % and C) high-resolution spectra (for C 1s, O 1s and N 1s).

To perform XPS studies the sample referred to as **PB50**, was cut into three samples of which two were protonated and only one was eventually loaded with AgNPs. The C 1s and O 1s high resolution spectra for all the three kind of samples showed easily recognizable features for C-C (284 eV), C=O (289 eV C 1s and 531.5 eV O 1s), C-N (533 eV). The N 1s spectrum showed clearly the tertiary amine group at 399 eV and a shoulder at 402 eV indicated that a minor fraction of the amine groups was in the protonated state. After soaking in dilute nitric acid, along with the 399 eV peak, this shoulder at 402 eV became more pronounced confirming that the protonation step was successful. In addition, a peak at 406 eV appeared which was assigned to the nitrate anion. This peak was underestimated, suggesting that some nitrate anions were stripped off by the high vacuum.

ADDITIONAL NOTES ON PAS TECHNIQUE AND RESULTS

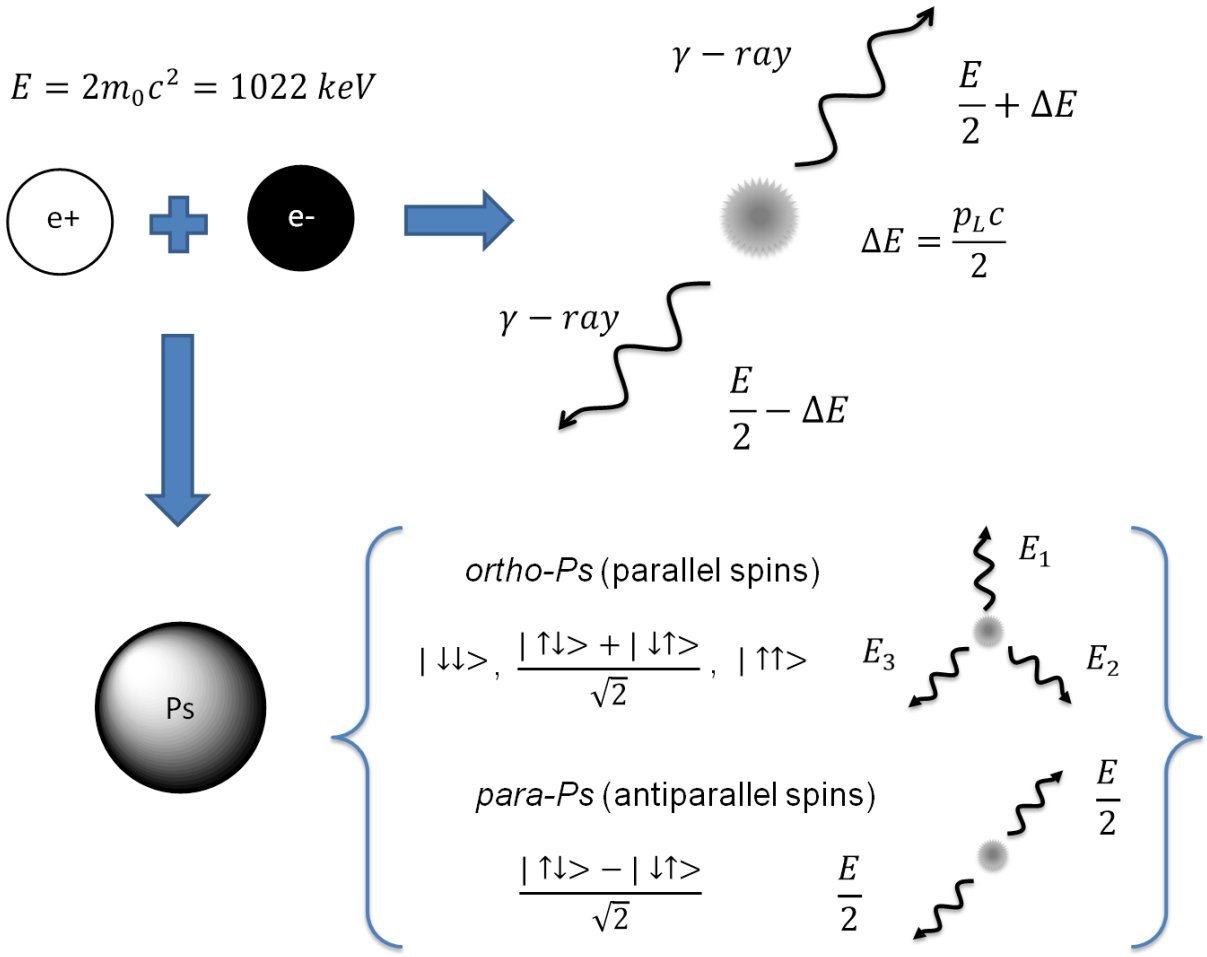

Scheme S2. Scheme of the electron-positron interaction. The positron can annihilate as a free positron with an electron of a material in two antiparallel gamma-rays of 511 keV (upper right sector). The gamma-ray energy is shifted by a quantity ΔE due to the Doppler effect; this quantity is proportional to the momentum of the electron–positron couple p_L along the gamma-rays direction. In cavities or free volumes positronium (Ps) can be formed (lower sector), following the spin selection rule, as ortho-Ps and para-Ps. The first annihilates in vacuum in three gamma-rays while the second in two gamma-rays. The Doppler shifts are not indicated because are rather small compared to the free annihilation process.

THE VEPAS BEAM

In order to perform thin film depth profile studies, i.e. to obtain a small penetration depth, the use of a positron beam is mandatory. A positron beam is made of monoenergetic ("slow") positrons that can be set to defined energies by simple linear accelerators. The VEPAS beam allows the tuning of the positron implantation energy from 0.1 to 20 keV. These energies allow to study thin films in the range of depth from the surface up to some microns, depending on the massive density of the studied material. The positrons are emitted by a ^{22}Na radioactive source and filtered by a moderator, *i.e.* a monocrystalline, [100]-oriented, W foil. With regard to Figure S7, the beam consists of two perpendicular tracks where electrostatic tubular lenses have been placed into a vacuum chamber (10^{-6}-10^{-8} mbar).

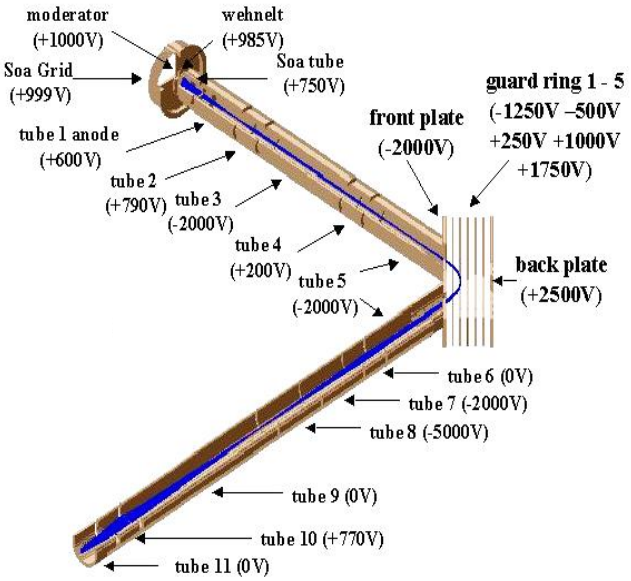

Figure S7. Design of the electrostatic optics of the VEPAS slow positron beam. The potentials correspond to the optics for positrons that arrive to the sample (focus point) with a kinetic energy of 1 keV. The positron trajectories represented in blue are simulated using SIMION 3D v7.0.[5]

The positrons are initially gathered through a series of electrodes, placed according to a modified design of a Soa gun, which potentials are optimized in order to bring to the first anode the highest number of positrons. The first track has to accelerate the beam and make it parallel. Since the sample should not come in direct contact with the positrons emitted by the source, next to the fifth electrostatic lens there is a deflection unity (bender), similar to an analyser with parallel flat faces, which bends the beam by 90°. Then, after the bender, there are three lenses. The first lens refocuses the beam, the second accelerates the beam, and the third, consisting of three electrodes, focuses the beam on the sample. The gamma radiation, that possesses the information of the annihilation process, is collected by two high-purity germanium detectors (HPGe) each one located at 4 cm to the sample.

The final kinetic energy of positrons corresponds to the potential difference between the sample and the moderator. Between the moderator and the sample there has to be a potential difference of at least 1 kV so as to have an high enough transport efficiency. To obtain implantation energies between 1 keV and 20 keV, the tension of the whole apparatus must be increased until the eighth tube and, for the energy range between 0.1 keV and 1 keV, a potential applied to the sample between 0 and 0.9 kV is required.

CALCULATION OF THE POSITRON MEAN IMPLANTATION DEPTH (PAS)

The *S, W* and $F_{3\gamma}$ parameters are shown in Fig. S8 as a function of the positron implantation energy. This figure is an alternative of Fig. 2 presented in the article. It should be taken into account that the data correspond to samples with different densities whatever if the brushes are loaded or not loaded with silver nanoparticles. It should also be noted that the *S* and *W* parameters were normalized to the value of the silicon substrate ($S = S_m/S_{Si}$ and $W = W_m/W_{Si}$, where $S_{Si} \approx 0.543$, $W_{Si} \approx 0.112$ and S_m and W_m are the measured values). As is apparent from the graph, the *S* and *W* parameters are nearly complementary. Figure S9 shows the *W* parameter *vs S* parameter plot with more details. It is possible to follow the evolution of both parameters from the surface up to the silicon substrate (black squares). There are two additional "poles" in the protonated films with and without silver nanoparticles loading which are related to para-positronium formation and to the interface (red squares, see main text). Note that bumps appear in the evolutions of the *S* parameter in Fig. S8 at about 1-2 keV (valleys in the *W* parameter evolutions) if silver is present into the brushes. These bumps are attributed mainly to p-Ps formation and positron annihilation at the Ag nanoparticles surface and not to positrons annihilating into the silver nanoparticles (see the main text). In this sense, the silver "pole" in Fig. S9 (orange symbol) does not correspond to the direction of the *S* parameter bumps (*W* parameter valleys), *i.e.* to p-Ps formation.

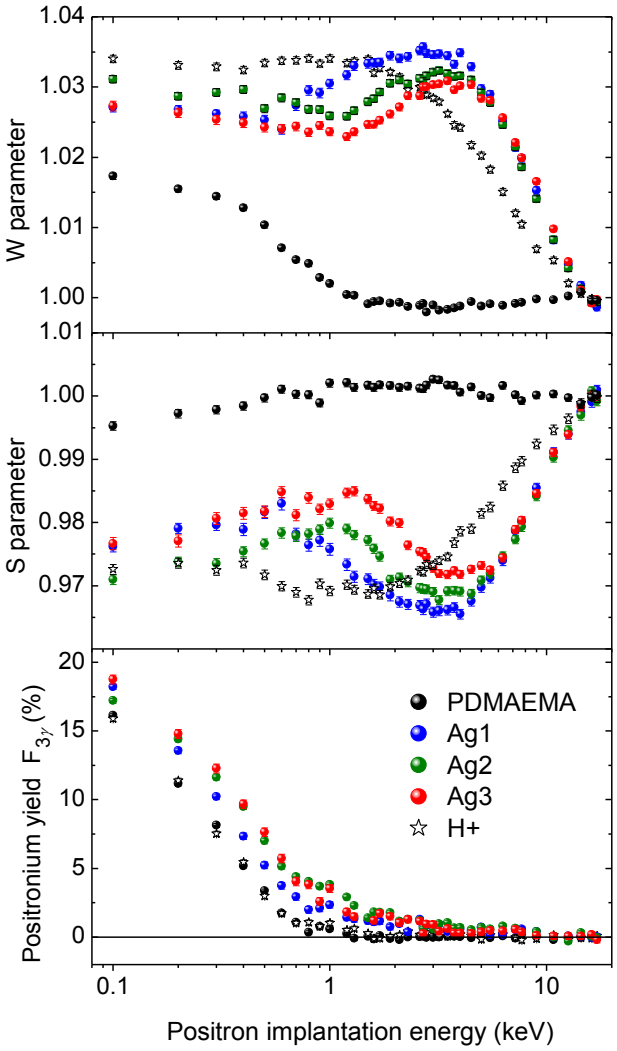

Figure S8. *S*, *W* and $F_{3\gamma}$ parameters as a function of the positron implantation energy for pristine, protonated and silver nanoparticles-loaded PDMAEMA brushes grown on silicon substrate.

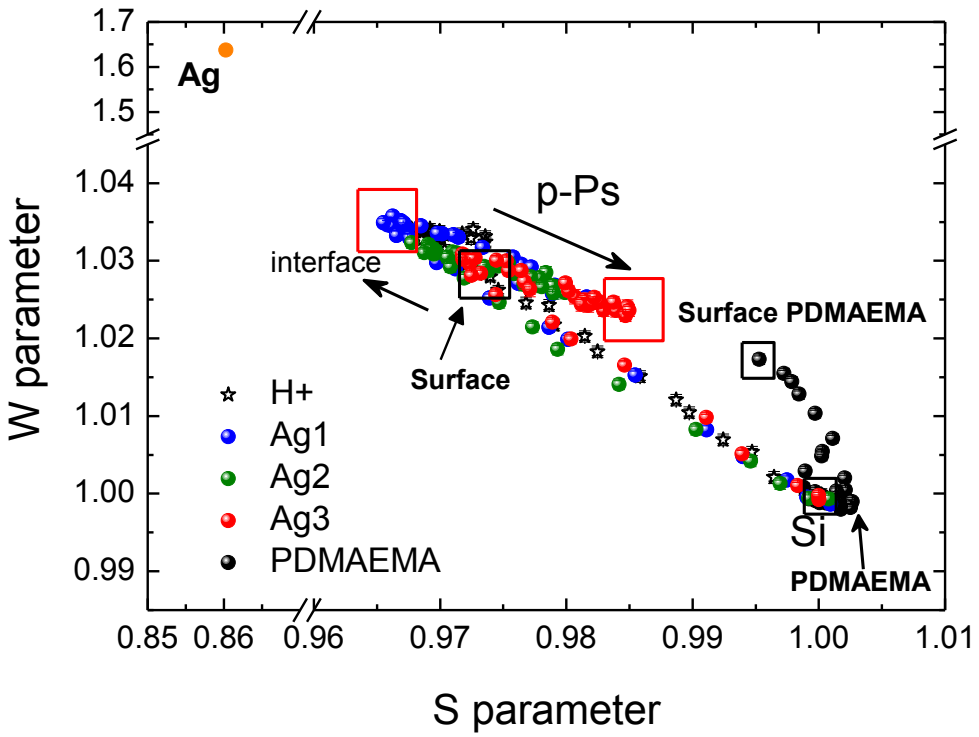

Figure S9. *W* parameter vs. *S* parameter plot (data of Fig. S8).

The mean implantation depth of the positrons as a function of the positron implantation energy was calculated using a numeric algorithm based on the Makhov implantation profile. This calculation is essential to represent and compare data of samples with the same nature but containing layers with different densities. The probability of a positron, having an implantation energy *E*, to penetrate to a depth *z* into a sample with density *d* is given by the so-called Makhov profile:[6]

$$P(z,E) = \frac{mz^{m-1}}{z_0^m} e^{\left[-\left(\frac{z}{z_0}\right)^m\right]} \quad \text{(S2)}$$

with

$$z_0 = \frac{AE^r}{d\,\Gamma\left(1+\frac{1}{m}\right)} \quad \text{(S3)}$$

where *m*, *r* and *A* are empirical parameters and Γ is the gamma function. The most accepted values of these parameters are m = 2, r = 1.6 and A = 40 μg cm^{-2} keV^{-r} (when z is expressed in nm).[7]

For the monodimensional probability distribution function in eq. S2, the mean implantation depth is given by:

$$\bar{z} = \int_0^\infty zP(z,E)\,dz = \frac{AE^r}{d} \tag{S4}$$

The PDMAEMA samples which PAS results are showed in Fig. 2 (article) were modeled as composed of two layers: i) the brushes layer characterized by the thickness indirectly measured with XRR and the density estimated with VEPFIT and ii) the silicon, a semi-infinite layer of 2.33 g cm^{-3} density.

The Makhov profiles for the bilayered samples have been approximated with:

$$P(z,E) = \begin{cases} \frac{mz^{m-1}}{z_{0,1}^m} e^{\left[-\left(\frac{z}{z_{0,1}}\right)^m\right]}, & z \le z_1 \\ \frac{m(z-z_1+\delta z)^{m-1}}{z_{0,2}^m} e^{\left[-\left(\frac{z-z_1+\delta z}{z_{0,2}}\right)^m\right]}, & z > z_1 \end{cases} \tag{S5}$$

where z_1 is the thickness of the first layer, $z_{0,1}$and $z_{0,2}$ are calculated according to eq. S3 for each layer and δz is a depth for which the following relation is valid:

$$P = \int_0^{z_1} P_1(z,E)dz = \int_0^{\delta z} P_2(z,E)dz \tag{S6}$$

In Fig. S10 the mean implantation depth trends are represented as a function of the positron implantation energy for the PDMAEMA sample obtained by using the method described above.

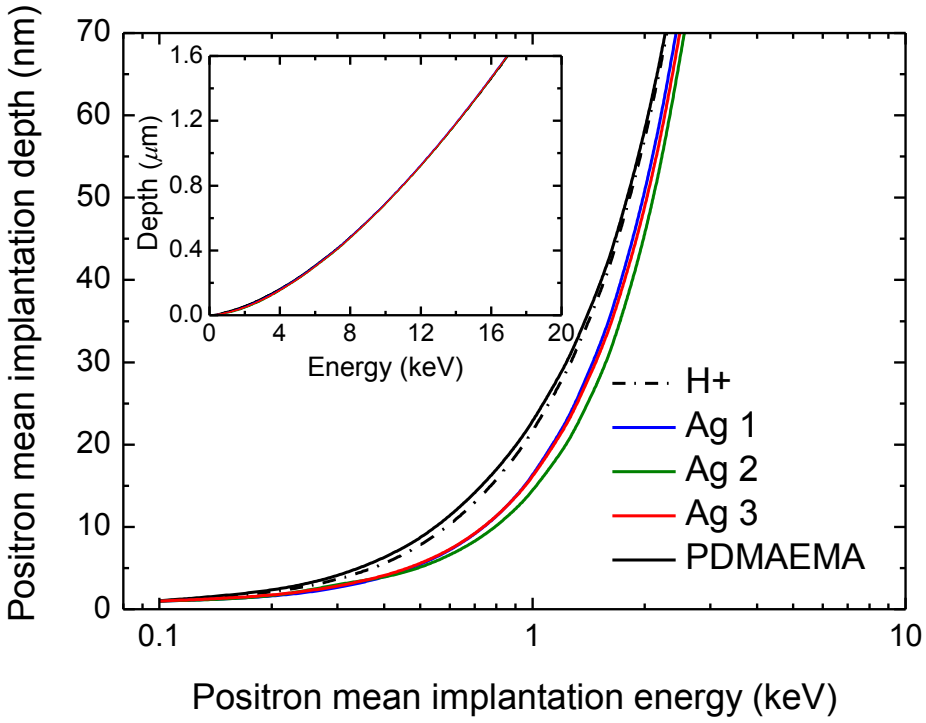

Figure S10. Calculated positron mean implantation depth as a function of the kinetic implantation energy.

REFERENCES

1) Panzarasa, G.; Soliveri, G.; Sparnacci, K.; Ardizzone, S. *Chem. Commun.* **2015**, *51*, 7313–7316.

2) Panzarasa, G.; Soliveri, G.; Ardizzone, S.; Sparnacci, K. *Mater. Today. Proc.* **2015**, *2*(8), 4183–4189.

3) Panzarasa, G. *J. Chem. Educ.* **2014**, *91*, 696–700.

4) Soliveri, G.; Pifferi, V.; Panzarasa, G.; Ardizzone, S.; Cappelletti, G.; Meroni, D.; Sparnacci, K.; Falciola, L. *Analyst* **2015**, *140*, 1486–1494.

5) SIMION®, Scientific Instrument Services, Inc. http://www.simion.com/

6) Makhov, A. F. *Soviet Physics-Solid State* **1961**, *2*, 1934–1941.

7) Vehanen, A.; Saarinen, K.; Hautojärvi, P.; Huomo, H. *Phys. Rev. B.* **1987**, *35*, 4606–4610.